Ultrafast Dynamics of Small Clusters on the Time Scale of Nuclear Motion

Michael Hartmann,[†] Andreas Heidenreich,[‡] Jiří Pittner,[†] Vlasta Bonačić-Koutecký,[†] and Joshua Jortner*,[‡]

Walther-Nernst-Institut für Physikalische und Theoretische Chemie, Humboldt-Universität zu Berlin, Bunsenstrasse 1, D-10117 Berlin, Germany, and School of Chemistry, Tel Aviv University, Tel Aviv 69978, Israel

Received: November 21, 1997; In Final Form: February 9, 1998

We present a theoretical study of the multistate dynamics of the $Ag_3^-/Ag_3/Ag_3^+$ system on the time scale of nuclear motion, as explored by femtosecond pump−probe negative ion-to neutral-to positive ion (NENEPO) spectroscopy. The dynamics of the Ag_3 cluster initiated from its linear transition state involves configurational relaxation, intracluster collision, and onset of IVR, resonant and dissipative IVR and vibrational equilibration, whose time scales were determined. Our analysis reveals that theory is essential for the elucidation of the rich dynamic information regarding geometrical change, completion of IVR, and vibrational coherence effects in the NENEPO femtosecond signals.

1. Introduction

Novel and interesting facets of ultrafast cluster, condensed phase, and biophysical (adiabatic and nonadiabatic) dynamics can be triggered by charge separation, expansion, localization, or transfer. Typical examples in finite and infinite systems involve multistate nuclear dynamics in $Ag_3^-/Ag_3/Ag_3^+$ negative ion-to neutral-to positive ion (NENEPO) spectroscopy of small clusters,[1−4] the fate of Rydberg excitations resulting in a "bubble" or "spring" formation in mixed rare-gas Xe* Ar_N clusters,[5,6] relaxation of an excess electron via "bubble" formation in simple dense fluids, e.g., liquid He, Ne, or H_2,[7,8] vibrational coherence effects impact-induced in clusters[5,6,9−11] or in the condensed phase,[12−15] and ultrafast electron transfer in solution[16,17] or in a protein medium.[18]

Clusters are of considerable interest in the context of ultrafast nuclear dynamics for several reasons: (1) The number of degrees of freedom and the density of states can be continuously varied by changing the clusters size.[19,20] (2) The nuclear dynamics allows for a separation of time scales between high-frequency (intramolecular) and low-frequency (intermolecular) motions in clusters.[21] (3) Dynamic cluster size effects allow for the investigation of the "transition" from resonant dynamics to dissipative dynamics by increasing the cluster size.[22]

In this paper we report on multistate femtosecond dynamics of small clusters on the time scales of nuclear motion. The elucidation of nuclear dynamics triggered by vertical electronic−vibrational excitation or ionization pertains to time-resolved transition state spectroscopy and dynamics.[23−30]

2. NENEPO Femtosecond Dynamics

Wolf et al.,[1] Berry et al.,[2] and Leisner and Wöste[3] pioneered the NENEPO pump−probe femtosecond spectroscopy to explore the nuclear dynamics of the $Ag_3^-/Ag_3/Ag_3^+$ system. In these experiments a transient linear Ag_3 cluster in its ground electronic state $^2\Sigma_u^+$ was prepared by a one-photon photodetachment of linear Ag_3^- ($^1\Sigma_g^+$) and its time evolution from linear Ag_3 ($^2\Sigma_u^+$) to triangular (B_2^2) nuclear configuration was interrogated by a delayed ionizing pulse via two-photon ionization. A recent significant extension of the experimental study of Ag_3^- by the NENEPO pump−probe method, utilizing two-color excitation and sensitive ion and electron detection, was presented by Boo et al.[4]

The original interpretation provided by Wolf et al.[1] of their experimental results was based on the assumption that the temporal shape of the signals is determined by the time-dependent Franck−Condon vibrational overlap integrals between the potential energy surfaces (PESs) of Ag_3 and Ag_3^+ during the structural relaxation process from the linear initial to the bent equilibrium structure of Ag_3. Lineberger et al.[4] invoked the additional effects of the acceleration of the nuclear wave packet of Ag_3 toward the triangular configuration with the maximization of the Franck−Condon factors between the PES of Ag_3 and Ag_3^+ in the vicinity of the triangular configuration. Some model calculations[31,32] of the time dependence of the ionization potential of Ag_3 induced by structural response seem to confirm the gross features of the experimentalists' interpretation.[1−4] Our theoretical studies[33,34] of the nuclear dynamics and pump−probe femtosecond spectroscopy of the $Ag_3^-/Ag_3/Ag_3^+$ system reveal that the experimental time-resolved NENEPO signal must be supplemented by theory to elucidate the rich dynamic information for this system with providing essential complementary information for time-resolved experimental spectroscopy.

In this paper, we shall address the following issues regarding the nuclear dynamics of the Ag_3 cluster initiated by vertical photodetachment of Ag_3^- to the linear transition state:

(1) Is the bending structural change sufficient for the understanding of the ultrafast dynamics? We shall show that in addition to configurational relaxation to the triangular configuration, sequential intracluster vibrational relaxation (IVR) processes dominate the intracluster dynamics.

(2) What are the intracluster IVR processes? These involve intracluster collisions, the onset of IVR, resonant and dissipative IVR, and vibrational equilibration, whose time scales were determined.

[†] Humboldt-Universität zu Berlin.
[‡] Tel Aviv University.

S1089-5639(98)00309-0 CCC: $15.00
Published on Web 04/22/1998

(3) Can dissipative IVR be exhibited in a "small" cluster? Indeed, our simulations demonstrate that dissipative IVR and vibrational equilibration are already exhibited in a three-atom system at excess vibrational energies of ≈0.4 eV, corresponding to the equilibrium temperature of ≈1400 K.

(4) How are the features of the dynamics manifested in the experimental NENEPO signals? We show how geometrical change and completion of IVR can be identified in the femtosecond pump−probe signals.

(5) Can vibrational coherence effects be revealed? We show under which interrogation conditions vibrational coherence induced by the intracluster collisions can be identified in the NENEPO signal.

3. Methodology

We present a theoretical study of the NENEPO femtosecond pump−probe signals and of the underlying nuclear dynamics of the Ag_3^-, Ag_3, and Ag_3^+ system. The bases for our molecular dynamics trajectory simulations, which are used for the calculations of the pump−probe signals, are precomputed grids of the three potential energy surfaces, which we have obtained from high-quality ab initio CI and coupled cluster quantum chemistry calculations. The calculations of the three ground-state potential energy surfaces (PES) of Ag_3^-, Ag_3, and Ag_3^+ were carried out by using a relativistic one-electron effective core potential accounting for core−valence correlation (RECP−CVC) together with the atomic basis set which was developed for the investigation of structural properties of neutral and charged silver clusters.[35,36] The use of RECP−CVC allowed for the full CI treatment of the three- and two-electron systems Ag_3 and Ag_3^+, while for Ag_3^-, the computationally less demanding CCSD(T) method has been used instead. As already known from previous work[35,36] the global minima of the anionic, neutral, and cationic silver trimers assume linear, obtuse triangular, and equilateral triangular structures, respectively.

Figure 1 presents two-dimensional contour plots of the PESs of the ground states of Ag_3^-, Ag_3, and Ag_3^+. The normal coordinates Q_s, Q_x, and Q_y of the Ag_3^+ cation are used to represent the PESs. Q_s, Q_x, and Q_y correspond to the symmetric stretching, the bending, and the antisymmetric stretching coordinate, respectively. The contour plots are given for two fixed values of Q_s, $Q_s = 2.73$ Å for the $Ag3^-/Ag_3$ (panels a,b) and $Q_s = 2.81$ Å for the Ag_3/Ag_3^+ surfaces (panels c,d). These values of Q_s correspond to the absolute minima on the PES for Ag_3^- and for Ag_3, respectively. Figure 1 manifests the relevant spatial region for the pump $Ag_3^- \rightarrow Ag_3$ vertical photodetachment (panels a,b) and for the probe $Ag_3 \rightarrow Ag_3^+$ vertical ionization during the relaxation on the Ag_3 PES (panels c,d). The most straightforward relevant information pertains to the energetics of the ionization process. The theoretical data for the vertical photodetachment energy (VDE_0) of Ag_3^- ($^1\Sigma_g^+$, $VDE_0 = 2.45$ eV) from its equilibrium nuclear configuration and the vertical photoionization potential (VIP) of linear Ag_3 ($^2\Sigma_u^+$, $VIP_{lin} = 6.67$ eV) and of the obtuse triangular (equilibrium) Ag_3 ($^2B_2$, $VIP_{triang} = 5.73$ eV) provide central information on the choice of the pump and the probe photon energies. Regarding the pump process, the experimental data were obtained for the one-photon pump energies $E_{pu} = 2.95-3.13$ eV,[1−4] which considerably exceed $VDE_0 = 2.45$ eV. In this context the information for reliable Franck−Condon factors between realistic potential energy surfaces is significant. On the basis of the information for the rather narrow distribution of the Franck−Condon factors for the vertical photodetachment energies (VDE) of Ag_3^- (shown in Figure 2 at 300 K) we infer

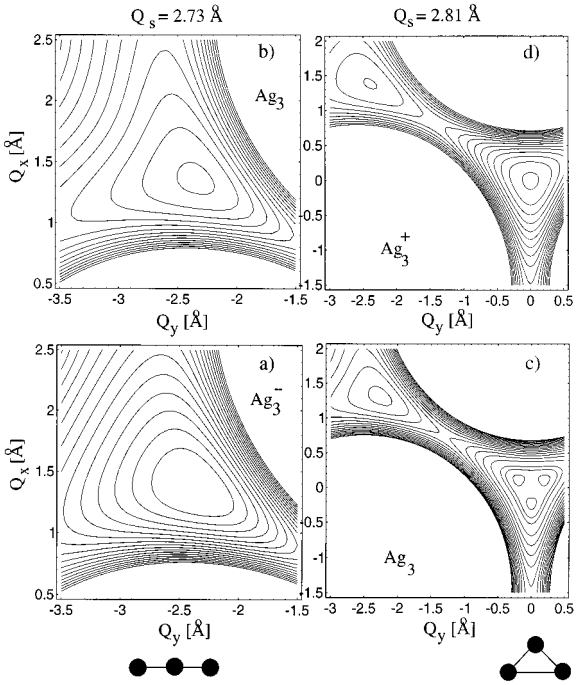

Figure 1. Q_x, Q_y contour plots of the ground electronic PESs of Ag_3^-, Ag_3, and Ag_3^+. (a, b) The PESs of Ag_3^- and Ag_3 for a fixed value of $Q_s = 2.73$ Å at the equilibrium geometry of the anion, showing the regions around the minimum of the anion (a) and of the saddle point of the neutral (b). (c, d) The PESs of Ag_3 and Ag_3^+ for a fixed value of $Q_s = 2.81$ Å, which corresponds to the equilibrium configuration of the neutral. Saddle points are located at $Q_x \approx 1.4$ Å, $Q_y \approx -2.5$ Å. The minimum of the Ag_3^+ cation is at $Q_x = 0$, $Q_y = 0$. The obtuse triangular equilibrium geometry of Ag_3 in the vicinity of $Q_x = 0$, $Q_y = 0$ is 3-fold degenerate due to the Jahn−Teller effect.

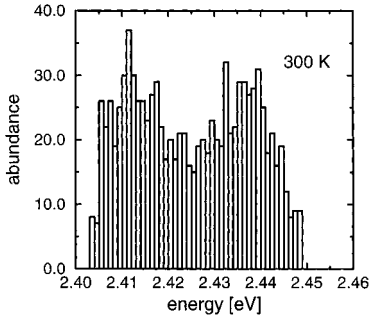

Figure 2. Histogram of the vertical detachment energies (VDEs) of the Ag_3^- anion at 300 K. The upper limit 2.45 eV of the distribution is temperature independent, as it corresponds to the VDE_0 value of the equilibrium nuclear configuration of the anion.

that in the energy range $E_{pu} = 2.95-3.13$ eV the excess photon energy above the VDE is transferred to the kinetic energy of the ejected electron, while the initial vibrational distribution of Ag_3 is essentially determined by the thermally averaged vibrational overlap between Ag_3^- and Ag_3. Regarding the probe process with the two-photon probe energy E_{pr}, the energetics is limited by $VIP_{triang} \leq E_{pr} \leq VIP_{lin}$, characterizing the ionization probe detection window ($E_{pr} = 5.73-6.67$ eV) for the interrogation of the dynamics from the linear to the bent structure of Ag_3. It is apparent that meaningful theoretical information on energetics, Franck−Condon factors, and nuclear dynamics requires the use of reliable high-quality potential energy surfaces. Such information is crucial for the exploration of the time-resolved spectroscopy and dynamics of covalent, semiconductor, and metallic clusters.

We have utilized the Wigner representation of the density matrix introduced by Li, Fang, and Martens[37] to simulate the pump−probe signal, using classical molecular dynamics trajectory calculations on "good" ab initio potential surfaces of the $Ag_3^-/Ag_3/Ag_3^+$ system. We have simulated pump−probe signals under two different experimental conditions:

(1) Zero kinetic energy (ZEKE) of the emitted photoelectrons induced by the pump and the probe pulse. This experimental situation corresponds to NENEPO-ZEKE spectroscopy. The transient photoionization signal is

$$S[t_d] \propto \int d\mathbf{q}_0\, d\mathbf{p}_0 \int_0^\infty d\tau_1 \exp\left\{-\frac{(\tau_1 - t_d)^2}{\sigma_{pu}^2 + \sigma_{pr}^2}\right\} \exp\left\{-\frac{\sigma_{pr}^2}{\hbar^2}[E_{pr} - V_{21}(\mathbf{q}_1(\tau_1; \mathbf{q}_0))]^2\right\} \exp\left\{-\frac{\sigma_{pu}^2}{\hbar^2}[E_{pu} - V_{10}(\mathbf{q}_0)]^2\right\} P_{00}(\mathbf{q}_0, \mathbf{q}_0) \quad (1)$$

where t_d is the delay time between the temporal peaks of the Gaussian pump (pu) and probe (pr) pulses. E_{pu} and E_{pr} are the pump and the probe energies $\hbar\omega_{pu}$ and $2\hbar\omega_{pr}$, respectively, assuming for the latter a nonresonant character of the two-photon probe ionization. V_{10} and V_{21} are the energy gaps between the adiabatic PES of Ag_3^- and Ag_3 and of Ag_3 and Ag_3^+, respectively. $P_{00}(\mathbf{q}_0, \mathbf{p}_0)$ represents the nuclear occupation density on the Ag_3^- PES.

(2) Measurement of photoelectrons of arbitrary energy yields the energy-averaged NENEPO signals, which are given by

$$S[t_d] \propto \int d\mathbf{q}_0\, d\mathbf{p}_0 \int_0^\infty d\tau_1 \exp\left\{-\frac{(\tau_1 - t_d)^2}{\sigma_{pu}^2 + \sigma_{pr}^2}\right\} \int_0^\infty dE_2 \times \exp\left\{-\frac{\sigma_{pr}^2}{\hbar^2}[E_{pr} - V_{21}(\mathbf{q}_1(\tau_1; \mathbf{q}_0)) - E_2]^2\right\} \int_0^\infty dE_0 \exp\left\{-\frac{\sigma_{pu}^2}{\hbar^2}[E_{pu} - V_{10}(\mathbf{q}_0) - E_0]^2\right\} P_{00}(\mathbf{q}_0, \mathbf{p}_0) \quad (2)$$

Here the density of states in the ionization continuum is taken to be energy independent. The NENEPO experimental method,[1−4] which interrogates the total electron or ion yield, corresponds to this case.

From eqs 1 and 2 for the pump−probe photoionization signals the following picture emerges. Initially, the cluster is prepared in the ground electronic state 0 with the corresponding Wigner distribution $P_{00}(\boldsymbol{q_0}, \boldsymbol{p_0})$. $P_{00}(\boldsymbol{q_0}, \boldsymbol{p_0})$ is sampled from a long-time classical trajectory on the Ag_3^- anion PES for a given temperature. This initial phase space density ("initial ensemble") is spectrally filtered by the pump process to state 1 by the third Gaussian of eqs 1 and 2, respectively, i.e., each sampled phase space point $\boldsymbol{q_0}, \boldsymbol{p_0}$ assumes a spectral weighting factor. Subsequently, the filtered initial ensemble is classically propagated on the PES of the Ag_3 neutral (state 1) and is spectrally filtered again by the delayed ionization to state 2. This is expressed by the second Gaussian in the eqs 1 and 2. The total time resolution of the signal is determined by the pump−probe correlation function given by the first Gaussians in eqs 1 and 2. We found[34] that for sufficiently short laser pulses ($\sigma_{pu} \leq 100$ fs) the influence of the pump step on the temporal profile of the NENEPO-ZEKE and NENEPO signal is not very pronounced for the $Ag_3^-/Ag_3/Ag_3^+$ system. Accordingly, in what follows we shall present only results for $\sigma_{pu} = 0$, implying that the spectral filtering in the pump step is disregarded and that the total time resolution is somewhat enhanced. As we are interested in the interpretation of the experimental NENEPO signals[1−4] for $E_{pu} = 2.95-3.13$ eV, which considerably exceed VDE_0 (the upper limit of the distribution in Figure 2), this approach is adequate. The results of the complete pump−probe simulations will be given elsewhere.[34]

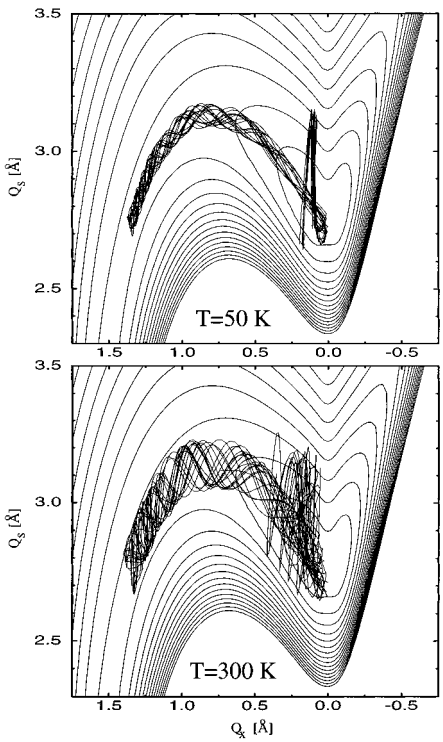

Figure 3. Bunches of trajectories of the 50 and 300 K ensemble projected on a Q_x, Q_s contour plot of the potential energy surface of Ag_3. Each bunch consists of 20 trajectories of 1.2-ps duration. The trajectories have been selected at random from the entire ensembles of 1000 trajectories.

4. Intracluster Collision, Onset, Evolution, and Completion of IVR

Information on the dynamics of configurational relaxation and onset of IVR was obtained from bunches of trajectories of 1.2 ps projected on a Q_s, Q_x contour plot ($Q_y = 0$) of the neutral Ag_3 PES. Figure 3 shows two bunches of trajectories of the 50 and 300 K initial ensemble. The time evolution of the system starts from the linear configuration around $Q_s = 2.7$ Å and $Q_x = 1.37$ Å in the flat region of the saddle point. With increasing time the system runs down the valley toward the potential minimum and becomes more bent. At the closest approach of the terminal atoms, which is located in the Jahn−Teller region around $Q_s = 2.7$ Å and $Q_x = 0.1$ Å, a strong repulsion sets in, resulting in the reflection of the terminal atoms. This reaching of the turning point on the PES corresponds to an intracluster collision. Up to the intracluster collision no significant IVR from the bending mode takes place. For the 50 K ensemble (upper panel), the intracluster collision induces a sharp reflection of the system from a motion along the Q_x bending coordinate to a motion along the Q_s stretching coordinate. For the 300 K ensemble (lower panel), the trajectories also assume a Q_x component after the collision.

The time scales for configurational relaxation, onset, evolution, and completion of IVR were inferred from the ensemble-averaged kinetic energy decomposed into normal modes. Figure 4 portrays this analysis for the 300 K ensemble with the characteristic times being marked on the panels. From these results we infer the following:

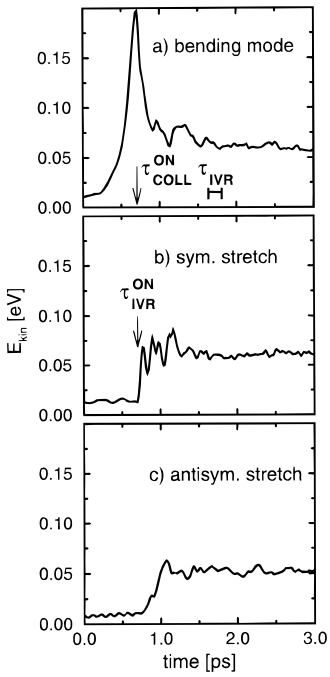

Figure 4. Time evolution of the kinetic energy in the normal modes of Ag_3 following the pump excitation of the 300 K initial ensemble. The kinetic energies of the normal modes were obtained as averages over the entire ensembles of 1000 trajectories. The characteristic times τ^{ON}_{COLL} (peak of E_{kin} in the bending mode), τ^{ON}_{IVR} (onset of the rise of E_{kin} in the symmetric stretching mode), and τ_{IVR} (temporal range of the completion of IVR) are marked in the panels.

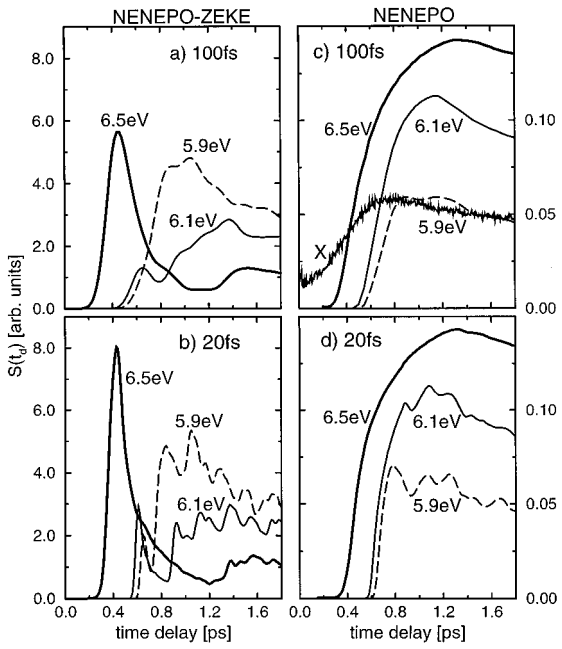

Figure 5. Simulated NENEPO-ZEKE (a, b) and NENEPO (c, d) probe signals for the 300 K initial ensemble. The probe energies E_{pr} are indicated at each curve and the pulse durations σ_{pr} are indicated in each panel. The simulated signals in panels a−d are shown as solid and dashed curves. The experimental signal (marked by X) of Wolf et al.[1] at $E_{pr} = 5.90$ eV is reproduced in panel c.

(1) The initial configurational relaxation across the bending coordinate prevails on the time scale $0-\tau^{ON}_{COLL}$, where τ^{ON}_{COLL} is the intramolecular collision time. The values of τ^{ON}_{COLL} were inferred from the peak of the kinetic energy in the bending mode.

(2) The intramolecular collision time is $\tau^{ON}_{COLL} = 710$ fs.

(3) The onset τ^{ON}_{IVR} is inferred from the threshold of the rise of the kinetic energy of the symmetric stretching mode. The τ^{ON}_{IVR} value coincides with the corresponding τ^{ON}_{COLL}, clearly showing that IVR is induced by the intramolecular collision.

(4) The IVR process is sequential, i.e., bending mode → symmetric stretching mode → antisymmetric stretching mode.

(5) The time evolution of the kinetic energy in the bending mode reveals dissipative IVR, while the 50 K ensemble (not shown) reveals some resonance effects.

(6) The time τ_{IVR} for the completion of IVR is manifested by the saturation and equipartition of the kinetic energy in all three modes, indicating vibrational equilibration. The IVR process is complete on the time scale $\tau_{IVR} \approx 1.6-1.8$ ps. It is important to emphasize that dissipative IVR, leading to the equilibration of the ensemble, prevails in a "small" triatomic system (with similar vibrational frequencies). An interesting question pertains to long recurrence times for the system, which are considerably beyond the experimentally relevant time regime.

(7) For the 50 K initial ensemble, the characteristic times τ^{ON}_{COLL}, τ^{ON}_{IVR}, and τ_{IVR} are all delayed by ≈250 fs relative to the corresponding time scales of the 300 K initial ensemble. The increase of these characteristic times with decreasing anion temperature reflects the lower initial velocities along the bending coordinate at the lower temperature.

It is gratifying that the details of the nuclear dynamics of a small system at a finite temperature can be elucidated, distinguishing between sequential processes of configurational changes (along the bending coordinate), intramolecular collision, the onset and evolution of IVR, and vibrational equilibration.

5. Femtosecond Pump−Probe Signals. Confrontation between Theory and Experiment

The interrogation of the nuclear dynamics by pump−probe spectroscopy requires the examination of the NENEPO-ZEKE signals, eq 1, and NENEPO signals, eq 2, for the two-photon ionization of Ag_3 (Figure 5). The information emerging from the NENEPO-ZEKE signals can be quantified in terms of the following observables: (i) the incubation time t_{INC} for the onset of the signal; (ii) the time t_M for the maximum of the signal, (iii) the onset t_L of the long-time behavior of the signal, i.e., when the signal is smoothed down to a constant level. In Figure 6a we summarize the temporal observables together with the characteristic times obtained from the nuclear dynamics. From the NENEPO-ZEKE data we infer the following:

(1) The incubation times are all shorter than the collision times, i.e., $t_{INC} \leq \tau^{ON}_{COLL} \simeq \tau^{ON}_{IVR}$. Accordingly, the incubation times (for all values of E_{pr}) probe the configurational change across the bending coordinate.

(2) The decrease of t_{INC} with increasing E_{pr} is due to the earlier arrival of the bending Ag_3 system to the probe time window.

(3) For high values of E_{pr} (≃6.5 eV) with an early onset of the probe time window, the hierarchy of the time scales is $t_{INC} \leq t_M \leq \tau^{ON}_{COLL} \simeq \tau^{ON}_{IVR}$. Under these circumstances a major part of the signal reflects dynamics prior to the intracluster collision, i.e., IVR-free dynamics. The NENEPO-ZEKE signal represents the time evolution of the configurational change across the bending coordinate. The temporal rise and fall of the signal reflects the front and tail of the phase space density along the bending coordinate, respectively. The temporal peak of the signal, t_M, corresponds to an obtuse triangular geometry with a

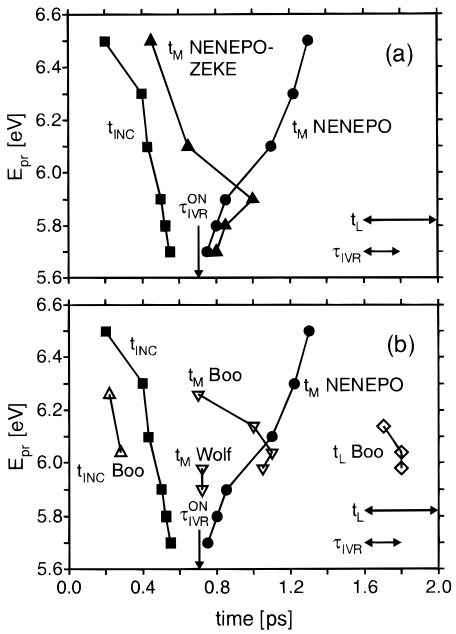

Figure 6. Summary and comparison of the simulated and experimental characteristic time scales of the neutral Ag_3 for different values of the probe energy (E_{pr}). (a) The simulated data. The characteristic times of the NENEPO and NENEPO-ZEKE signals, i.e., the incubation times t_{INC}, the times t_M at which the signals assume their maximum intensity, and the time t_L at which the signals reflect equilibration, are shown together with the onset τ_{IVR}^{ON} and the completeness τ_{IVR} of IVR. Horizontal arrows represent intervals of t_L and τ_{IVR} since they can be only approximately specified. The data for t_{INC} and for t_L are identical for the NENEPO-ZEKE and NENEPO signals. The data for t_M are different for the two types of signals, as marked by the curves. (b) A comparison of the simulated NENEPO signals (filled symbols) with the experimental data (open symbols) of Wolf et al.[1] and Boo et al.[4] The data points in (a) and (b) are connected by straight lines to guide the eye.

bond angle of ≈120° as compared to 180° for the initial geometry of the Ag_3^- anion and 68° for the equilibrium geometry of the neutral Ag_3.

(4) For low values of E_{pr} (i.e., 5.8−6.0 eV) the value of t_M for the NENEPO-ZEKE signal is larger, so that the hierarchy of the time scales is $t_{INC} \leq \tau_{COLL}^{ON} \leq t_M$. The probed dynamics until t_M is now much richer with the signal for $t_{INC} \leq t \leq \tau_{COLL}^{ON}$ reflecting structural bending prior to IVR, while on the time scale $\tau_{COLL}^{ON} \leq t \leq t_M$ the IVR occurs.

(5) At low E_{pr} (≤5.90 eV), t_M for the NENEPO-ZEKE signal is in the range $\tau_{IVR}^{ON} \leq t_M \leq \tau_{IVR}$.

(6) The time t_L, at which the NENEPO-ZEKE signal has smoothed down to its long-time constant level, measures the IVR time, i.e., $t_L = \tau_{IVR}$. Of course, t_L is nearly independent of E_{pr}.

The present experimental measurements of the NENEPO signals[1−4] involve the monitoring of the entire electron or positive ion yield, so that the NENEPO-ZEKE signals are integrated over the nearly constant density of continuum states of the emitted photoelectron, Figure 5c,d. Accordingly, details of the NENEPO-ZEKE signal are averaged out in part. The following features (Figure 6a) of the NENEPO signals as compared to the NENEPO-ZEKE signals should be noted:

(1) The incubation times are practically identical for the NENEPO-ZEKE and for the NENEPO signals. Accordingly, features (1) and (2) of the t_{INC} for NENEPO-ZEKE signals hold also for the NENEPO signals; i.e., the incubation times of the NENEPO signals also decrease with increasing E_{pr} and always precede the intracluster collisions.

(2) There is a quantitative and qualitative difference between the t_M data and their E_{pr} dependence for the NENEPO and for the NENEPO-ZEKE signals. For high E_{pr} (≈6.50 eV) values the peak of the NENEPO signal is exhibited at considerably longer times than the corresponding NENEPO-ZEKE signal. Thus when configurational bending dynamics is solely probed, the accumulative continuum of the signal results in considerable information loss. Only for low values of E_{pr} (5.8−6.0 eV) the averaging effects on t_M are not pronounced.

(3) For larger E_{pr} the peak of the NENEPO signal is exhibited at $t_M \lesssim \tau_{IVR}$, providing a lower limit for τ_{IVR}.

(4) The temporal onset t_L for the constant signal is practically equal for the NENEPO and for the NENEPO-ZEKE signals, providing a measurement for τ_{IVR}.

(5) The effect of the spectral filtering is smeared out, so that the temporal profile of the signal is nearly independent of E_{pu}.

From the foregoing analysis it is apparent that theoretical information is crucial for the elucidation of the experimental femtosecond pump−probe signals.[1−4] Proceeding to the comparison between our simulations and experiment, we use the data of the calculated NENEPO signals for the 300 K ensemble with the probing pulse length of 100 fs. The gross features of the experimental NENEPO signals[1−4] are reasonably well reproduced by our simulations (Figure 5c). The experimental data of Wolf et al.[1] at short delay times show an earlier rise smearing out the onset predicted by us, the discrepancy may be due to high-order (four-photon) direct ionization of Ag_3^- to Ag_3^+ by the pump pulse. The experimental results of Boo et al.[4] clearly exhibit the signal onset. We proceed now to a detailed confrontation between theory and experiment. The data extracted from the experimental signals of Wolf et al.[1] and Boo et al.[4] have been summarized in Figure 6b together with the simulated values at the initial Ag_3^- temperature of 300 K. This is approximately the temperature in the work of Wolf et al.,[1] while the anion temperature in the work of Boo et al.[4] is ≤100 K (due to their liquid nitrogen-cooled ion source and supersonic expansion). The temperature effects on the pump−probe NENEPO signals are quite significant, e.g., at 50 K the t_{INC} values are higher by 200−300 fs relative to 300 K. Our simulations cannot explain the differences between the experimental data of Wolf et al.[1] and of Boo et al.[4] (Figure 6). Accordingly, at the present stage we refrain from addressing the temperature effects. From the simulated and experimental data we conclude the following:

(1) From the work of Boo et al.[4] the experimental incubation times for $E_{pr} = 6.04$ eV and $E_{pr} = 6.26$ eV are in overall agreement with our simulations. In the signals of Wolf et al.[1] for the probe energies of 5.90 and 5.98 eV the incubation times are smeared out, presumably due to high-order multiphoton excitation of the anion.

(2) The experimental data for the times t_M of the peak maxima do not form a consistent picture. While the two data points of Wolf et al.[1] are at ≈700 fs, three of the data points of Boo et al.[4] at 5.98−6.14 eV are at ≈1000 fs, and a further data point for $E_{pr} = 6.26$ eV is at ≈700 fs. Our simulations for the NENEPO signals predict an increase of t_M with increasing E_{pr}. This trend is not exhibited by the experimental data, although four out of six data points can be considered to be in satisfactory agreement with the simulated t_M values.

(3) The three experimental t_L values of Boo et al.[4] for $E_{pr} =$ 5.98, 6.04, and 6.14 eV are in the range 1.7−1.8 ps, being in good agreement with our simulations of t_L and with the values of τ_{IVR}.

Our theoretical analysis predicts some new features of the dynamics which were not yet subjected to an experimental test.

(1) NENEPO-ZEKE Signals. The pump−probe femtosecond spectra with NENEPO-ZEKE detection will provide useful novel information for the separation between configurational relaxation (high E_{pr}) and IVR (lower E_{pr}) dynamics. This difficult experiment will provide a critical scrutiny of the dynamics.

(2) Initial Ensemble Temperature. The dependence of the nuclear dynamics manifested in NENEPO signals on the initial Ag_3^- ensemble temperature will be of interest. This will require the control of the Ag_3^- temperature by proper cooling or by infrared laser heating.

(3) Vibrational Coherence. The utilization of shorter (σ_{pu} = 20 fs) probe pulses will provide novel information on vibrational coherence effects predicted by us at 300 K. As apparent from Figure 5 for the 300 K ensemble, in the IVR regime the signals reveal oscillatory features at probe energies of 5.90 and 6.10 eV, indicating the signature of vibrational coherence induced by intracluster collisions. In contrast, the 50 K ensemble does not show marked vibrational coherence.[34] The analysis of this counterintuitive result in terms of energy gap oscillations will be given elsewhere.[34] The temporal spacing of the peaks is not equidistant and lies in the range 100−150 fs (Figure 5). The quantum beat pattern of the ensemble-average signal manifests the participation of the stretching modes (harmonic vibrational period of the symmetric and antisymmetric stretching modes: 193 and 295 fs, respectively). This constitutes another example of vibrational coherence induced by intracluster collision, which manifests a general phenomenon in the realm of ultrafast cluster dynamics. Analogous phenomena pertain to cage effects in the dissociation of I_2 in Ar_N clusters[9−11] and impact induced vibrational coherence induced by "cage" and "bubble" formation around extravalence Rydberg excitation in Xe^*Ar_N clusters.[5,6]

Our theoretical treatment has to be extended in several directions. First, the inclusion of nonadiabatic effects in the vicinity of the minimum of the neutral triangular structure, where the crossing of the potential surfaces $^2B_2$ and $^2A_1$ occurs, requires a more elaborate treatment. Second, in our approach the presence of intermediate states for which resonance effects can occur at some probe energies has not been considered. Such resonance effects are expected to modify both the intensity dependence on the probe energy as well as the time profile of the signal. Third, the extension of the theoretical exploration of multistate nuclear dynamics for NENEPO signals of larger systems will modify the temporal interplay between configurational relaxation and IVR dynamics, manifesting IVR at shorter time scales than for the "small" Ag_3^- system studied herein.

Acknowledgment. We are grateful to Prof. L. Wöste, Dr. T. Leisner, Prof. R. S. Berry, and Prof. W. C. Lineberger for stimulating discussions and for prepublication information. This research was supported by the Deutsche Forschungsgemeinschaft SFB 337 and BO627/14-1 at Humboldt University, by the Volkswagen Foundation, and by the German-Israeli Binational James Franck Program at Tel Aviv University.

References and Notes

(1) Wolf, S.; Sommerer, G.; Rutz, S.; Schreiber, E.; Leisner, T.; Wöste, L.; Berry, R. S. *Phys. Rev. Lett.* **1995**, *74*, 4177.
(2) Berry, R. S.; Bonacic-Koutecky, V.; Gaus, J.; Leisner, Th.; Manz, J.; Reischl-Lenz, B.; Ruppe, H.; Rutz, S.; Schreiber, E.; Vajda, S.; de Vivie-Riedle, R.; Wolf, S.; Wöste, L. *Adv. Chem. Phys.* **1997**, *101*, 101.
(3) Leisner, T.; Wöste, L., to be published.
(4) Boo, D. W.; Ozaki, Y.; Andersen, L. H.; Lineberger, W. C. *J. Phys. Chem. A* **1997**, *101*, 6687.
(5) Jortner, J. In *Femtochemistry*; Chergui, M., Ed.; World Scientific: Singapore, 1996; p 15.
(6) Goldberg, A.; Jortner, J. *J. Chem. Phys.* **1997**, *107*, 8994.
(7) Rosenblit, M.; Jortner, J. *Phys. Rev. Lett.* **1995**, *75*, 4079.
(8) Rosenblit, M.; Jortner, J. *J. Phys. Chem. A* **1997**, *101*, 751.
(9) Lineau, C.; Zewail, A. H. *J. Chim. Phys.* **1995**, *92*, 566.
(10) Papanikolas, J. M.; Vorsa, V.; Nadal, M. E.; Campagnola, P. J.; Buchenau, H. K.; Lineberger, W. C. *J. Chem. Phys.* **1993**, *99*, 8733.
(11) Papanikolas, J. M.; Maslen, P. E.; Parson, R. *J. Chem. Phys.* **1995**, *102*, 2452.
(12) (a) Wang, J.-K.; Liu, Q.; Zewail, A. H. *J. Phys. Chem.* **1995**, *99*, 11309. (b) Liu, Q.; Wang, J.-K.; Zewail, A. H. *J. Phys. Chem.* **1995**, 11321.
(13) Li, Z.; Zadoyan, R.; Apkarian, V. A.; Martens, C. C. *J. Phys. Chem.* **1995**, *99*, 7453.
(14) Wynne, K.; Reid, G. D.; Hochstrasser, R. M. *J. Chem. Phys.* **1996**, *105*, 2287.
(15) Bixon, M.; Jortner, J. *J. Chem. Phys.* **1997**, *101*, 1470.
(16) Seel, M.; Engleitner, S.; Zinth, W. *Chem. Phys. Lett.*, **1997**, *275*, 363.
(17) Pal, H.; Nagasawa, Y.; Tominaga, K.; Yoshihara, K. *J. Phys. Chem.* **1996**, *100*, 11964.
(18) Bixon, M.; Jortner, J. Electron Transfer via Bridges. *J. Chem. Phys.*, in press.
(19) Jortner, J. *Z. Phys. D* **1992**, *24*, 247.
(20) Jortner, J. *J. Chim. Phys.* **1995**, *92*, 205.
(21) Jortner, J.; Levine, R. D. *Isr. J. Chem.* **1990**, *30*, 207.
(22) Scharf, D.; Jortner, J.; Landman, U. *J. Chem. Phys.* **1988**, *88*, 4273.
(23) Mokhtari, A.; Cong, P.; Herek, J. L.; Zewail, A. H. *Nature* **1990**, *348*, 225.
(24) Dantus, M.; Bowman, R. M.; Gruebele, M.; Zewail, A. H. *J. Chem. Phys.* **1989**, *91*, 7437.
(25) Weaver, A.; Metz, R. B.; Bradforth, S. E.; Neumark, D. M. *J. Chem. Phys.* **1990**, *93*, 5352.
(26) Metz, R. B.; Neumark, D. M. *J. Chem. Phys.* **1992**, *97*, 962.
(27) Neumark, D. M. *Acc. Chem. Res.* **1993**, *26*, 33.
(28) Burnett, S. M.; Stevens, A. E.; Feigerle, C. S.; Lineberger, W. C. *Chem. Phys. Lett.* **1983**, *100*, 124.
(29) Ervin, K. M.; Ho, J.; Lineberger, W. C. *J. Chem. Phys.* **1989**, *91*, 5974.
(30) Wenthold, P. G.; Hrovat, D. A.; Borden, W. T.; Lineberger, W. C. *Science* **1996**, *272*, 1456.
(31) Jeschke, H. O.; Garcia, M. E.; Bennemann, K. H. *J. Phys. B* **1996**, *29*, L545.
(32) Jeschke, H. O.; Garcia, M. E.; Bennemann, K. H. *Phys. Rev. A* **1996**, *54*, R4601.
(33) (a) Hartmann, M.; Bonačić-Koutecký, V. Presented at the *Mixed Classical-Quantum Mechanical Systems Meeting*; Dresden; Oct 1996. (b) Heidenreich, A.; Jortner, J.; Hartmann, M.; Pittner, J.; Bonačić-Koutecký, V. Presented at the *James-Franck Symposium*; Ein Gedi; Jan 1997. (c) Hartmann, M.; Heidenreich, A.; Pittner, J.; Bonačić-Koutecký, V.; Jortner, J. Presented at the *Informal Cluster Workshop*; Berlin; May 1997.
(34) Hartmann, M.; Pittner, J.; Bonačić-Koutecký, V.; Heidenreich, A.; Jortner, J. *J. Chem. Phys.* **1998**, *108*, 3096.
(35) Bonačić-Koutecký, V.; Cespiva, L.; Fantucci, P.; Koutecky, J. *J. Chem. Phys.* **1993**, *98*, 7981.
(36) Bonačić-Koutecký, V.; Cespiva, L.; Fantucci, P.; Pittner, J.; Koutecky, J. *J. Chem. Phys.* **1994**, *100*, 490.
(37) Li, Z.; Fang, J.-Y.; Martens, C. C. *J. Chem. Phys.* **1996**, *104*, 6919.